Acta Cryst. (1994). A**50**, 98–106

The Diffraction Patterns of Crystals with Layer Defects

BY R. BERLINER

Research Reactor Center, University of Missouri–Columbia, Columbia, MO 65211, *USA*

AND R. J. GOODING

Department of Physics, Queens University, Kingston, Ontario K7L 3N6, Canada

(*Received* 1 *March* 1993; *accepted* 23 *July* 1993)

Abstract

A method for the calculation of X-ray and neutron diffraction profiles of crystals with layer defects is described. Averages over a computer model of a configurational ensemble of crystallites with defects are used to define the scattering cross section. The method easily accommodates the modeling of complex defect geometries or correlations. Diffracted intensity profiles for the Ni_xAl_{1-x} $(5, \bar{2})$ monoclinic martensite, trigonal polytypes and body-centered-cubic crystals are presented as examples.

1. Introduction

Many crystalline materials exist in nature in imperfect forms, incorporating various kinds of chemical and structural defects. A common defect is the stacking fault – a variation of the layer order or deviation of the real crystal from the pattern of layers that characterizes the perfect crystal. Stacking faults are known to have a considerable effect on the diffraction patterns obtained from neutron, X-ray or electron diffraction experiments. Substantial discrepancies between the observed pattern and the results expected from a naïve application of Bragg's law can arise. These effects include diffraction-peak broadening, diffuse scattering, streaking, diffraction-peak-position shifts and intensity modulation.

The study of stacking-fault defects has a long history. The earliest theoretical efforts extend back to the 1930s (Landau, 1937; Lifschitz, 1937, 1939), with contributions from many prominent workers in the intervening time. The work of Hendricks & Teller (1942), Wilson (1941, 1949) and Jagodzinski (1949) has been particularly influential. Discussion of the effects of various crystalline imperfections on diffraction can be found in a number of basic texts on X-ray (Guinier, 1963; Warren, 1969) and neutron diffraction (Bacon, 1975; Krivoglaz, 1969) and a comprehensive review of the subject is available (Welberry, 1985).

The fundamental mathematical relations required for the description of a crystal incorporating layer defects have long been known and have been presented in a number of forms. Two different mathematical approaches, the difference-equation method (Wilson, 1941) and the matrix method (Hendricks & Teller, 1942), have been attractive to theoretical investigators, although few results have been obtained for real crystals because of the complexity of the necessary computations. Application of these methods has been limited to structures containing elementary layer defects, that is twin or deformation faults, in simple systems.

This paper illustrates a different method for the calculation of neutron diffraction patterns from polycrystalline and single-crystal specimens that incorporate various kinds of layer defects. It is an extension of an effort to understand the diffraction patterns that result from displacive phase transitions in the alkali metals lithium (Berliner & Werner, 1986) and sodium (Berliner, Fajen, Smith & Hitterman, 1989; Berliner, Smith, Copley & Trivisonno, 1992). An earlier and more restrictive description of diffraction from crystals with layer defects was provided in the context of that work.

The idea that underlies the method described here is that the average structure for the defective crystal, suitable for the calculation of the diffraction pattern, can be directly formed by averaging over a statistical configurational ensemble of crystallites, 'grown by the computer'. Complex defects and defect correlations can be introduced by altering the rules that the computer uses to assemble the individual crystallites that make up the ensemble. In the case of polycrystalline material, the phsical meaning of the statistical ensemble is clear – it corresponds to the set of crystallites appropriately oriented for diffraction of the incident radiation into the detector. For a single crystal with layer defects (or a coarse-grained polycrystal), elements of the ensemble are seen as representing different regions of the specimen, each of these regions of a size determined by the range of correlations permitted by the defect density.

The plan of presentation of these results is first to recast the (three-dimensional) general relations for the diffraction of radiation from a crystal into a simpler one-dimensional form. It will be seen that this is appropriate for a crystal with layer defects and considerably simplifies the problem of calculating the defect-crystal diffracted intensities. The underlying structure of the perfect crystal can then be specified algorithmically and a rule for introducing defects defined. The layer order or the orientation of the individual layers is maintained for each crystallite and used to calculate the averages that define the diffracted intensity of the ensemble. As an example, the effect of stacking faults in Ni_xAl_{1-x} following its martensitic transformation is analyzed. In addition, the analogous analysis for the classic cases of stacking faults in trigonal polytypes and body-centered-cubic crystals is presented.

2. Diffracted-intensity calculation

The basic relations that govern the diffraction of neutrons from crystalline materials are presented here as the basis for the material that follows. The X-ray case can be obtained by using the appropriate **Q** and polarization-dependent scattering amplitudes in the equations.

Consider a crystal composed of N_c equally spaced identical layers.† The layers each form a perfect two-dimensional lattice in the a and b directions but will be supposed to exhibit stacking disorder along the c axis – each layer being displaced relative to its neighbor parallel to the ab plane. The scattering cross section for neutrons incident on this kind of specimen may be written as

$$\mathrm{d}\sigma/\mathrm{d}\Omega = \sum_{nn'}\sum_{\gamma\gamma'}\sum_{\rho\rho'} b_\rho \exp(-i\mathbf{Q}\cdot\mathbf{r}_{n\gamma\rho}) b^*_{\rho'} \times \exp(i\mathbf{Q}\cdot\mathbf{r}_{n'\gamma'\rho'}), \quad (1)$$

where $\mathbf{r}_{n\gamma\rho} = \mathbf{R}_n + \mathbf{r}_\gamma + \mathbf{r}_\rho$ is the position of the ρth atom in the γth (planar) unit cell of the nth layer. The quantity b_ρ is the neutron scattering length for the atom at the position $\mathbf{r}_{n\gamma\rho}$ and $\mathbf{Q} = 2\pi(h\mathbf{a}^* + k\mathbf{b}^* + l\mathbf{c}^*)$, with the standard definitions of the reciprocal-lattice vectors $\mathbf{a}^*$ and $\mathbf{b}^*$. For convenience, we define $\mathbf{c}^*$ in terms of the interlayer separation and not the c-axis lattice parameter; consequently, l is not restricted to integer values.

The sums over ρ and ρ' yield the layer unit-cell structure factor $f(\mathbf{Q})$ and

$$\mathrm{d}\sigma/\mathrm{d}\Omega = \sum_{nn'}\sum_{\gamma\gamma'} f(\mathbf{Q})\exp(-i\mathbf{Q}\cdot\mathbf{r}_{n\gamma}) f(\mathbf{Q})^* \exp(i\mathbf{Q}\cdot\mathbf{r}_{n'\gamma'}), \quad (2)$$

with $\mathbf{r}_{n\gamma} = \mathbf{R}_n + \mathbf{r}_\gamma$. Since the layers are themselves two-dimensional lattices, $\mathbf{r}_\gamma = m_1\mathbf{a} + m_2\mathbf{b}$, with m_1 and m_2 integers, and $\mathbf{R}_n$ represents the displacement of the nth layer relative to the origin. If the linear dimensions of a layer are large, *viz* N_a, $N_b \gg 1$, substitution into (2) and summation over m_1, m_2, m_1' and m_2' gives

$$\mathrm{d}\sigma/\mathrm{d}\Omega = |f(\mathbf{Q})|^2 N_a N_b \sum_{nn'} \exp[i\mathbf{Q}\cdot(\mathbf{R}_{n'} - \mathbf{R}_n)]. \quad (3)$$

Equation (3) can be put in a more convenient form if we let $n' = n + \delta$ and rearrange the double sum:

$$\mathrm{d}\sigma/\mathrm{d}\Omega = |f(\mathbf{Q})|^2 N_a N_b \Bigg(N_c + \sum_{\delta=1}^{N_c-1}\sum_{n=1}^{N_c-\delta} \{\exp[i\mathbf{Q}\cdot(\mathbf{R}_{n+\delta} - \mathbf{R}_n)] + \text{c.c.}\}\Bigg), \quad (4)$$

where the inner sum is now over all pairs of layers separated by a distance $\delta\mathbf{c}$, $\mathbf{c}$ is the interlayer separation and c.c. refers to the complex conjugate of the preceding term. The inner sum is now seen to be the sum of the exponential for all layers separated by δ layers.

3. Ni_xAl_{1-x}

We now consider an example system and demonstrate how to calculate the diffraction pattern from a crystal with layer defects. Our modeling will serve to illustrate our technique; however, the subject we discuss here remains an outstanding problem, requiring analysis more sophisticated than that appearing here.

Ni_xAl_{1-x} with $0.60 < x < 0.64$ has a CsCl structure at high temperature and accommodates excess Ni atoms on the Al sublattice. On cooling, the material martensitically transforms to a seven-layered monoclinic structure known as the $7M$ phase.† In the martensite, the monoclinic a and b axes lie near to the cubic [101] and [010] directions and the c axis is nearly parallel to the cubic [101] direction. The low-temperature martensite was studied with X-rays by Martynov, Enami, Khandros, Nenno & Tkachenko (1983), who suggested that the structure could be understood as the stacking of cubic (101) planes, each plane sheared an amount u in the monoclinic a direction with respect to the previous layer. From the pattern of diffraction-peak intensities, it was determined that the shears exhibited a $(5, \bar{2})$ pattern, that is five successive

† Although the planes described by the indices $\{h,k,l\}$ are formally identical in any crystal system, these do not necessarily correspond to the layers most conveniently used to describe layer defects.

† The Ni_xAl_{1-x} martensite actually consists of a number of structural forms and embedded twin bands in addition to the $7M$ phase.

shears parallel to **a** followed by two shears in the opposite direction. Fig. 1 contains a representation of the Ni_xAl_{1-x} martensite structure.

The high-resolution neutron diffraction studies of Noda, Shapiro, Shirane, Yamada & Tanner (1990) and Shapiro, Yang, Noda, Tanner & Schryvers (1991) demonstrated that Ni_xAl_{1-x} becomes unstable as it is cooled. Phonon softening and diffuse scattering presage the appearance of a new phase at (approximately) the seven-layer periodicity observed. These authors found that the diffraction pattern from a single variant of the Ni_xAl_{1-x} martensite deviated from that expected for a $(5, \bar{2})$ layer stacking rule. They observed diffraction-peak broadening, peak-position shifts and peak splitting along $h0l$ lines. Then, by *assuming* an underlying perfect crystalline $7M$ state, they obtained the crystallographic parameters $a_m = 4.172$, $b_m = 2.690$ and $c_m = 14.450$ Å, with a monoclinic angle $\beta_m = 94.37°$, as the structural parameters of the new phase.

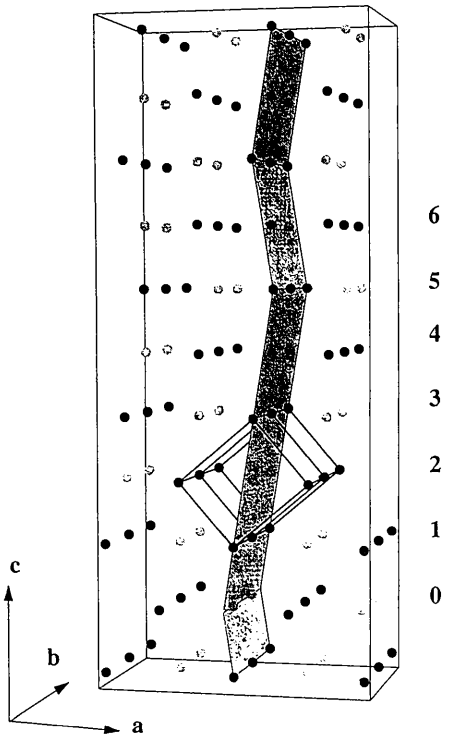

Fig. 1. The Ni_xAl_{1-x} martensite structure. Ten layers of the monoclinic crystal with Ni atoms denoted ● and Al atoms ◉ illustrate the shifting of the (former) cubic (101) planes by an amount u at each layer in the $(5, \bar{2})$ pattern. Two parallelepipeds marking atoms corresponding to two unit cells of the original cubic Ni_xAl_{1-x} structure have been outlined. The shadowed plane segments passing up the middle of the figure illustrate the transformation-induced distortion of the cubic $(10\bar{1})$ plane. The orientation of the orthorhombic coordinates used for the stacking-fault diffraction-profile calculation are shown. The layers corresponding to one monoclinic cell have been numbered.

Yamada, Noda & Fuchizake (1990) have proposed an Ni_xAl_{1-x} martensite structure incorporating regions with the same $(5, \bar{2})$ stacking sequence but two (slightly different) monoclinic angles. This work relies on the assumption of (nonlinear) stability of so-called periodon structures (Barsch & Krumhansl, 1988), a novel and yet poorly understood excitation. This analysis is in reasonable agreement with experiment. However, the presence of multiple structural variants* for the martensite phase, along with the accompanying disorder, make it reasonable to argue that anomalies in the diffraction patterns may result from layer defects frozen into the crystal by the transformation (the so-called accommodation problem).

In what follows, we use a simplified description of the NiAl structure, one that allows easy demonstration of the effect of layer defects on diffraction patterns. To be specific, we assume that, for the martensitic phase, successive cubic (101) planes are sheared in the manner described above. Then, there are a number of simple errors in the stacking sequence that could affect the diffraction pattern:

(1) Twin and deformation faults. These are the simplest stacking errors for the Ni_xAl_{1-x} martensite crystal. In the first case, the crystal would contain regions where the stacking sequence changed from $(5, \bar{2})$ to $(2, \bar{5})$. In the second case, the stacking order would be interrupted at some layer by a shear in the direction opposite to that prescribed by the $(5, \bar{2})$ stacking rule.

(2) Stacking variants. Sections of the martensite crystal might adopt a different stacking order. A layer stacking order corresponding to $(4, \bar{1}, 1, \bar{1})$ or $(3, \bar{1}, 2, \bar{1})$ would maintain the monoclinic angle but would be expected to change diffraction-peak intensities. Stackings that follow rules such as $(4, \bar{3})$, $(4, \bar{2})$, $(5, \bar{3})$ and so on will tend to alter the monoclinic angle and diffraction-peak positions and intensities.

In addition to the defects described above, more complex defect geometries, such as the 'double-twin' stacking fault observed in the alkali-metal martensites (Berliner *et al.*, 1989, 1992; Gooding, 1989; Prodanos & Gooding, unpublished) might be present.

The objective is to obtain the diffracted intensity for an oriented ensemble of Ni_xAl_{1-x} crystallites in terms of the reciprocal-space coordinates for comparison between different stacking-fault models and the experimental results. In this context, the monoclinic coordinates are inconvenient. Starting from the perfect $(5, \bar{2})$ crystal, stacking faults that change the

* Unless the degeneracy is broken in some fashion, crystallization of the low-temperature Ni_xAl_{1-x} martensite phase can occur along any of the six $\langle 110 \rangle$ directions of the CsCl high-temperature phase.

(average) monoclinic angle also change the direction and magnitude of the appropriate reciprocal-space coordinates. Therefore, orthorhombic coordinates will be used to describe the individual Ni_xAl_{1-x} crystallites. The orthorhombic a and b axes are the same as the corresponding monoclinic coordinates, while the interlayer spacing, $(c/7)\cos(\beta_m - \pi/4)$, will be used to define $\mathbf{c}^*$.

In these orthorhombic coordinates, the position of the nth layer for a general stacking of layers in the Ni_xAl_{1-x} martensite can be written as

$$\mathbf{R}_n = (\mathbf{a}/4)[1-(-1)^n] + ug_n\mathbf{a} + n\mathbf{c}, \qquad (5)$$

where the first term represents the gross alternation of atom positions that the martensite inherits from the cubic (101) planes, the second term accounts for the accumulated interlayer shear at layer n and the last term represents the displacement along the c axis. The value of the monoclinic angle and c-axis lattice parameter obtained by Noda *et al.* (1990) require that $u = 0.328$ Å. The quantity g_n tabulates the sequence of layer–layer shears that describe the stacking order.

Using the definition of $\mathbf{R}_n$ given in (5) and the standard representation of $\mathbf{Q}$, it is possible to rewrite the exponential in (4) as

$$\begin{aligned}
&\exp[i\mathbf{Q}\cdot(\mathbf{R}_{n'} - \mathbf{R}_n)] \\
&\quad = (-1)^h \exp\{2\pi i[hu(g_{n+\delta} - g_n) + \delta l]\} \qquad \delta \text{ odd} \\
&\exp[i\mathbf{Q}\cdot(\mathbf{R}_{n'} - \mathbf{R}_n)] \\
&\quad = \exp\{2\pi i[hu(g_{n+\delta} - g_n) + \delta l]\} \qquad \delta \text{ even.}
\end{aligned} \qquad (6)$$

From (4) and (6) and with the average over the ensemble of crystallites explicitly shown, the diffracted intensity for an Ni_xAl_{1-x} crystal with stacking faults is given by

$$\begin{aligned}
I(Q) = |f(\mathbf{Q})|^2 N_a N_b \Bigg(& N_c \\
& + (1/T)\Bigg\{ \sum_{\substack{\delta=2 \\ \text{even}}}^{N_c-1} \sum_{\text{trials}}^{T} \sum_{n=1}^{N_c-\delta} 2[\cos(2\pi hu\Delta g_{n,\delta}) \\
& \times \cos(2\pi\delta l) + \sin(2\pi hu\Delta g_{n,\delta}) \sin(2\pi\delta l)] \\
& + \sum_{\substack{\delta=1 \\ \text{odd}}}^{N_c-1} \sum_{\text{trials}}^{T} \sum_{n=1}^{N_c-\delta} 2(-1)^h [\cos(2\pi hu\Delta g_{n,\delta}) \\
& \times \cos(2\pi\delta l) + \sin(2\pi hu\Delta g_{n,\delta}) \sin(2\pi\delta l)] \Bigg\} \Bigg),
\end{aligned} \qquad (7)$$

where $\Delta g_{n,\delta} = (g_{\delta+n} - g_n)$.

The prescription for calculating the diffracted intensity profile for a perfect Ni_xAl_{1-x} crystal using (7) is

(1) Model the layer stacking by assembling the N_c layers according to the $(5, \bar{2})$ stacking rule. In practice, g_n is tabulated for the N_c layers that correspond to a single crystallite of the ensemble.

(2) Compute the sum of $[\cos(2\pi hu\Delta g_{n,\delta}) + \sin(2\pi hu\Delta g_{n,\delta})]$ for all sets of layer pairs separated by δ layers.

(3) Repeat steps (1) and (2) for each of T crystallites in the ensemble. As each crystallite is 'grown', the sum computed in step (2) is maintained so at the end the global sum over all layers for all the crystallites in the ensemble is obtained.

(4) Perform the sum over δ for the particular value of $\mathbf{Q}$, *i.e.* h, k and l.

In order to introduce defects, the stacking of layers described in step (1) above can be changed. A deformation fault in the Ni_xAl_{1-x} martensite can be modeled as a change in the stacking rule so that, at a random place in the $(5, \bar{2})$ sequence, the plus (or minus) layer–layer shear becomes a minus (or plus). The accumulated interlayer shear g_n for the first 15 layers of a perfect $(5, \bar{2})$ sequence is displayed in Fig. 2(*a*), while g_n for a sequence with two deformation faults is shown in Fig. 2(*b*).

Fig. 3(*a*) contains the calculated intensity profile $I(l)$ along an $h = 4$, $k = 0$ line for an Ni_xAl_{1-x} crystal with randomly introduced (2% probability per layer) deformation faults. The perfect-crystal diffraction pattern is shown in Fig. 3(*b*). Both calculations are for an ensemble with $T = 100$ and $N_c = 200$, which has been empirically determined to be sufficient for the numerical averages to converge. The intensity is calculated along an $h0l$ line because of the well known fact that stacking-fault disorder of the planes parallel to the a and b directions manifests itself in the diffraction profile parallel to the c^* axis in reciprocal space. In Fig. 3(*b*), the diffraction peaks have been labeled with the standard monoclinic indices for comparison to the data of Fig. 4 of Noda *et al.* (1990).

The diffraction pattern for defects of any complexity can be studied, limited only by the willingness of the investigator to specify (and code) the rule for their insertion into the perfect-crystal stacking sequence. For instance, the model can be further refined by allowing the deformation-fault occurrence probability to be different at each layer. Also, in principle, one could allow for differing shifts (say $+u_1$ for shifts in the plus direction and $-u_2$ for those in the opposite direction). Fig. 2(*c*) shows g_n for 15 layers of the $(5, \bar{2})$ sequence where a fault occurs regularly at each seventh layer. This produces a new lattice with the $(6, \bar{1})$ stacking rule. In Figs. 3(*c*) to (*g*), the diffracted intensity is calculated along the $40l$

line for this defect with occurrence probabilities of 0.10, 0.25, 0.5, 0.75 and 1.0. In this fashion, the diffraction pattern for all intermediate states of order between a pure $(5, \bar{2})$ and a perfect $(6, \bar{1})$ can be obtained. In this sequence of calculations, the diffraction-peak positions systematically shift as the 'average' stacking order and consequent monoclinic angle change. In addition, the diffraction peaks broaden as the stacking-fault probability approaches 0.5 – this is where the disorder is greatest.

It is also possible to select models that will change the 'average' number of layers in the unit cell. Such models create diffraction-peak position shifts as well as changes in the number of peaks observed. It is not unusual to find some diffraction peaks strongly broadened or shifted while others are hardly affected as the stacking-fault insertion probability is varied.

The diffraction pattern appropriate to a polycrystal can be obtained from (7) by a two-step process. First, the intensity profile for crystallites with the reversed stacking order (twins) is given by $I(l_{\text{twin}}) = I(-l)$. The diffraction pattern in terms of the scattering angle 2θ is then simply given by the intersection of the sphere of reflection with the intensity profile $I_{\text{total}}(l) = I(l) + I(-l)$, which assumes an equal probability for the direct and twinned layer stackings in the polycrystalline sample. Note that, in the case of a polycrystal, the direct and twinned crystallites scatter incoherently. This is in contrast to the case of twin faults within a single crystal, discussed above, where the computation must properly account for the interference terms.

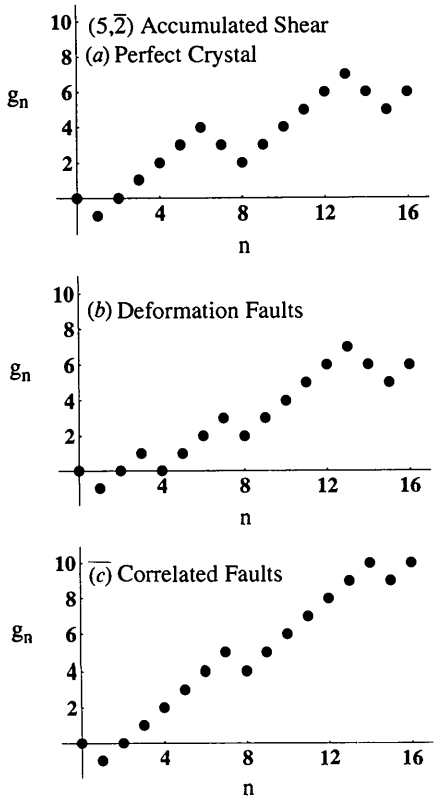

Fig. 2. Accumulated layer–layer shear index, g_n representing: (*a*) a perfect $(5, \bar{2})$ stacking; (*b*) a $(5, \bar{2})$ stacking with two deformation faults, one at $n = 4$ and the other at $n = 7$. Note that, in this case, the effects of these two faults cancel for $n > 8$. (*c*) A deformation fault that occurs at the same place (site 7) in each set of seven layers creates a new crystal structure. In this case, a $(6, \bar{1})$ stacking.

Calculation of the diffraction profile of the Ni_xAl_{1-x} martensite for a variety of layer defect types has not yet duplicated the pattern of intensities revealed by the neutron diffraction experiments of Noda *et al.* (1990). In particular, their observation that *h*0*l* diffraction peaks are shifted by differing amounts and directions, with respect to the perfect $(5, \bar{2})$ peak positions, has not been reproduced in these simulations and we conclude that the appropriate defect has not yet been identified. One may view our modeling as a method of using stacking faults to change randomly the local monoclinic angle without the unsubstantiated assumption of the stability of the periodon distortion. Additional computer modeling as well as some experimental investigations are still in progress.

4. Stacking faults in other crystal structures

The calculation of diffraction profiles for the Ni_xAl_{1-x} martensite provides a good example of the methods that would be used for the analysis of stacking faults in other crystal structures. This section briefly addresses additional examples: the classic cases of stacking faults in trigonal polytypes and on the (211) planes of body-centered-cubic crystals. These examples have been extensively analyzed both experimentally and theoretically and excellent summaries of the effects of simple faults on the diffraction profiles have been published (Welberry, 1985; Schwartz & Cohen, 1977; Barrett & Massalski, 1980). The material here is included because this method of modeling the defective crystalline state permits the consideration of more complex defects.

4.1. *Trigonal structures*

Viewed along the cubic [111] direction, the atoms in a single layer of a face-centered-cubic (f.c.c.) crystal form a two-dimensional trigonal lattice. In the perfect crystal, the atoms in successive layers occupy the well known *A*, *B*, *C* (or *A*, *C*, *B*) positions in sequence. If the atom positions alternate between two of these choices, say *A* and *B*, a hexagonal-close-packed (h.c.p.) lattice will result. The h.c.p. and f.c.c. crystal structures are dicusssed in nearly every standard work on condensed-matter physics and crystal-

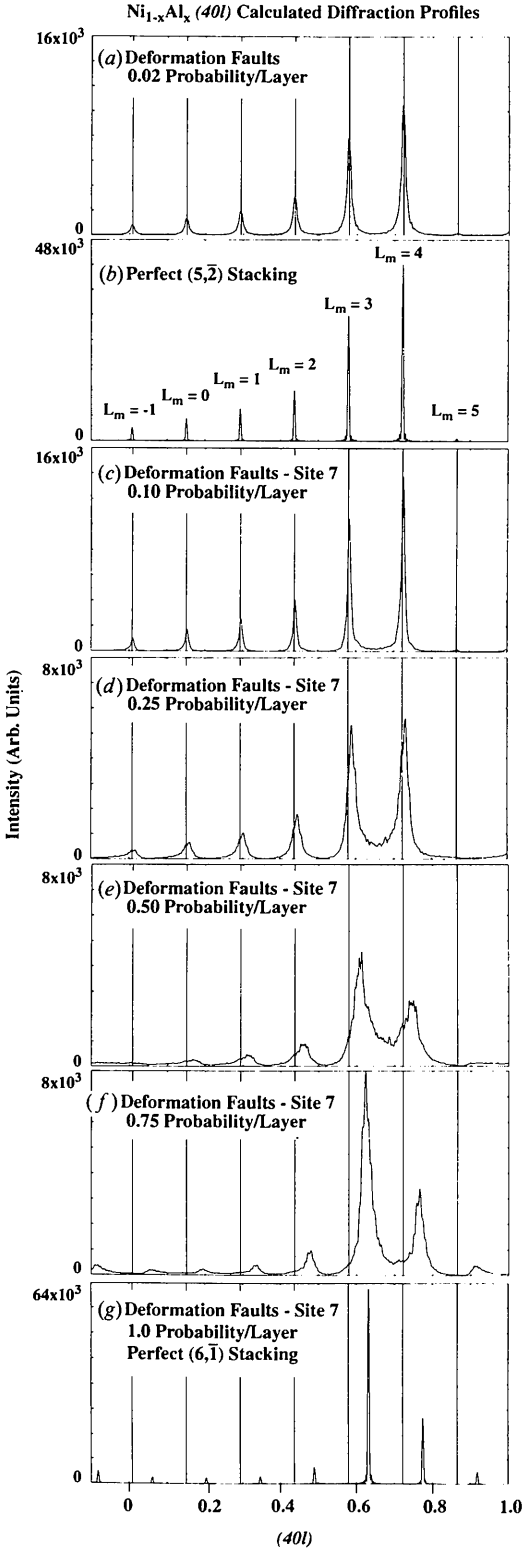

Fig. 3. Calculated diffraction patterns for the Ni_xAl_{1-x} martensite. All the profiles are calculated for an ensemble of 100 crystallites 200 layers long. The layers are assumed to be arbitrarily large in the transverse directions. (*a*) The 40*l* diffraction profile for a 0.02 deformation-fault probability at each layer. (*b*) The perfect (5, $\bar{2}$) stacking profile. The positions of the peaks have been labeled with the standard monoclinic indices. (*c*)–(*f*) Diffraction profiles for deformation-fault probabilities of 0.10, 0.25, 0.50, 0.75 at site 7 ($n = 6$ in Fig. 2*a*). (*g*) The diffraction profile for a site-7 deformation-fault probability of 1.0. This is a perfect crystal with (6, $\bar{1}$) stacking.

lography. What is less widely appreciated is that there are many other crystal structures built from the same motif. The number of unique close-packed stackings (polytypes) of trigonal layers is further discussed by Berliner & Werner (1986). A comprehensive treatment of the entire question of polytypes and their diffraction patterns is given by Verma & Krishna (1966). In addition to the variety of possible polytype crystal structures, polytypes support a rich array of topologically possible stacking faults. Some of the consequences of complex stacking faults in long-period rhombohedral polytypes were analyzed by Berliner *et al.* (1992).

A method for calculating stacking-fault-altered polycrystalline diffraction profiles in trigonal polytypes was derived by Berliner & Werner (1986) and the extension to single-crystal specimens was stated without proof by Berliner *et al.* (1989). A derivation of that result is presented here.

In the perfect f.c.c. crystal, atoms in successive layers occupy the *A*, *B*, *C* (or *A*, *C*, *B*) positions at

$$\begin{aligned} \mathbf{R}_A &= 0\mathbf{a} + 0\mathbf{b} \\ \mathbf{R}_B &= (\tfrac{2}{3})\mathbf{a} + (\tfrac{1}{3})\mathbf{b} \\ \mathbf{R}_C &= (\tfrac{1}{3})\mathbf{a} + (\tfrac{2}{3})\mathbf{b}. \end{aligned} \tag{8}$$

The position of the nth layer is then given by

$$\mathbf{R}_n = [(\tfrac{2}{3})\mathbf{a} + (\tfrac{1}{3})\mathbf{b})]g_n + n\mathbf{c}, \tag{9}$$

where $g_n = 0, 1, 2, 3, 4, \ldots$ for the *ABCAB*... stacking that characterizes a f.c.c. crystal. Equation (4) can then be written as

$$\mathrm{d}\sigma/\mathrm{d}\Omega = b^2 N_a N_b \left[N_c + \sum_{\delta=1}^{N_c-1} \sum_{n=1}^{N_c-\delta} (\exp\{2\pi i[(2h/3) + (k/3)]\Delta g_{\delta,n}\} \exp(2\pi i/\delta) + \text{c.c.}) \right], \tag{10}$$

where $\Delta g_{\delta,n} = g_{\delta+n} - g_n = \{0, \pm 1, \pm 2, \ldots\}$. For $\mathrm{mod}_3(\Delta g_{\delta,n}) = 0$, layers $n + \delta$ and n must be of the same type: *A*–*A*, *B*–*B* or *C*–*C*. When $\mathrm{mod}_3(\Delta g_{\delta,n}) = 1$, the layers $n + \delta$ and n are of the type *A*–*B*, *B*–*C* and *C*–*A*, while the case $\mathrm{mod}_3(\Delta g_{\delta,n}) = 2$ arises from *B*–*A*, *A*–*C*, *C*–*B*. With **Q** in reciprocal-space coordi-

nates, the cross section, (10), becomes

$$\begin{aligned}\mathrm{d}\sigma/\mathrm{d}\Omega = 2b^2N_aN_b\Big[& N_c \\ & + \sum_{\delta=1}^{N_c-1}[N_{AA}(\delta)+N_{BB}(\delta)+N_{CC}(\delta)] \\ & \times[\exp(2\pi i\delta l)+\text{c.c.})] \\ & + \sum_{\delta=1}^{N_c-1}[N_{AB}(\delta)+N_{BC}(\delta)+N_{CA}(\delta)] \\ & \times(\exp\{2\pi i[(2h/3)+(k/3)]\} \\ & \times\exp(2\pi i\delta l)+\text{c.c.}) \\ & + \sum_{\delta=1}^{N_c-1}[N_{BA}(\delta)+N_{CB}(\delta)+N_{AC}(\delta)] \\ & \times(\exp 4\pi i[(2h/3)+(k/3)] \\ & \times\exp(2\pi i\delta l)+\text{c.c.})\Big],\end{aligned} \tag{11}$$

where $N_{AA}(\delta)$, $N_{AB}(\delta)$, ..., $N_{CC}(\delta)$ are the numbers of pairs of layers of type AA, BB, ..., CC separated by a distance δ layers. After some algebra, the expression

$$\begin{aligned}\mathrm{d}\sigma/\mathrm{d}\Omega = b^2N_aN_b\Big[& N_c+\sum_{\delta=1}^{N_c-1}(2N_s(\delta)\cos(2\pi l) \\ & + 2[(N_c-\delta)-N_s(\delta)]\cos(2\pi\delta l) \\ & \times\cos\{2\pi[(h-k)/3]\}-N_D(\delta)\sin(2\pi\delta l) \\ & \times\sin\{2\pi[(h-k)/3]\})\Big]\end{aligned} \tag{12}$$

is obtained with

$$N_s(\delta) = N_{AA}(\delta)+N_{BB}(\delta)+N_{CC}(\delta) \tag{13}$$

and

$$\begin{aligned}N_D(\delta) = & [N_{BA}(\delta)-N_{AB}(\delta)]+[N_{AC}(\delta)-N_{CA}(\delta)] \\ & +[N_{CB}(\delta)-N_{BC}(\delta)],\end{aligned} \tag{14}$$

which is just the expression presented by Berliner *et al.* (1989). In the case of diffraction from a polycrystalline specimen with stacking faults, (12) adopts a particularly simple form (Berliner *et al.*, 1989), described earlier by Wilson (1941). There are extensive examples of the use of (12) by Berliner *et al.* (1989, 1992) for the case of double twin faults in the long-period rhombohedral polytypes.

4.2. *Faults in the* (211) *planes*

Through the 1950s and 1960s, various workers considered the problem of stacking faults in b.c.c. materials. The analyses of Guentert & Warren (1958) and Hirsch & Otte (1957) were applied to the broadening of the diffraction peaks in a variety of b.c.c. metals. They were applied to a variety of metal systems to identify the fault system for b.c.c. metals (Rothman & Cohen, 1971). In this section, the methods of this paper are applied to the problem of calculating the diffraction profile of a b.c.c. crystal with stacking faults.

The slip system in many b.c.c. crystal structures is along the (211) planes. Fig. 4 shows the atom positions for two successive (211) planes that comprise a b.c.c. crystal. The orientation of the cubic $[1\bar{1}0]$ and $[11\bar{1}]$ are also shown. In order to analyze the effect of stacking faults in this system, it is convenient, once again, to adopt orthorhombic coordinates:*

$$\begin{aligned}\mathbf{a}_o &= (\mathbf{a}_c+\mathbf{b}_c-\mathbf{c}_c)/2 \\ \mathbf{b}_o &= \mathbf{a}_c-\mathbf{b}_c \\ \mathbf{c}_o &= (\mathbf{a}_c+\mathbf{b}_c+2\mathbf{c}_c)/6,\end{aligned} \tag{15}$$

where the subscripts o and c identify the orthorhombic and cubic coordinates, respectively. Correspondence between the cubic, (HKL), and orthorhombic, (hkl), plane indices is obtained from (15) by replacing $\mathbf{a}_o$, $\mathbf{b}_o$, $\mathbf{c}_o$, by h, k, l and $\mathbf{a}_c$, $\mathbf{b}_c$, $\mathbf{c}_c$ by H, K, L, respectively.

In these orthorhombic coordinates, as the crystal is assembled by stacking the cubic (211)-plane layers, each of the layers is displaced in the transverse direction by the vector

$$\mathbf{R}_n = -(\mathbf{a}_o g_n)/3+(\mathbf{b}_o/4)[(-1)^n-1]+n\mathbf{c}_o, \tag{16}$$

where g_n is the accumulated shear of the nth layer. There are six separate orientations of the b.c.c. (211) layers before the pattern repeats. As with the f.c.c. crystal case, $g_n = 0, 1, 2, 3, \ldots$ for successive layers.

Equation (4) for the b.c.c. crystal can then be written as

$$\begin{aligned}\mathrm{d}\sigma/\mathrm{d}\Omega = b^2N_aN_b\Big\{ & N_c+(1/T) \\ & \times\sum_{\delta=1}^{N_c-1}\sum_{n=1}^{N_c-\delta}[\exp(2\pi i\{-(h/3)\Delta g_{\delta,n} \\ & +(k/4)[(-1)^{n+\delta}-(-1)^n]+\delta l\})+\text{c.c.}]\Big\},\end{aligned} \tag{17}$$

with the standard expansion of $\mathbf{Q}$. Expanding (17) and explicitly introducing the average over the

* This is the same as the orthorhombic coordinate system used by Hirsch & Otte (1957), except that the layer–layer separation along the c axis is used for the third coordinate instead of the lattice parameter.

ensemble, one obtains:

$$I(Q) = b^2 N_a N_b \Bigg[N_c + (1/T) \times \Bigg(\sum_{\substack{\delta=2 \\ \text{even}}}^{N_c-1} \sum_{\text{trials}}^{T} \sum_{n=1}^{N_c-\delta} 2\{\cos[2\pi(h/3)\Delta g_{\delta,n}] + \cos(2\pi\delta l)\sin[2\pi(h/3)\Delta g_{\delta,n}]\sin(2\pi\delta l)\} + \sum_{\substack{\delta=1 \\ \text{odd}}}^{N_c-1} \sum_{\text{trials}}^{T} \sum_{n=1}^{N_c-\delta} 2(-1)^h [\cos[2\pi(h/3)\Delta g_{\delta,n}] \times \cos(2\pi\delta l) + \sin[2\pi(h/3)\Delta g_{\delta,n}] \times \sin(2\pi\delta l)\} \Bigg) \Bigg], \quad (18)$$

which is quite similar to the expression obtained for Ni_xAl_{1-x}, (7), and can be evaluated using an analogous prescription. Equation (18) illustrates that only diffraction peaks with $h = 3p \pm 1$, $p = 0, 1, 2, \ldots$, are affected by layer defects.

Deformation faults of the b.c.c. (211) layer stacking can be modeled by jogs of g_n, as is the case in Ni_xAl_{1-x} or the trigonal polytypes. Figs. 5(*a*) and (*b*) show the calculated 10*l* diffraction profiles for b.c.c. crystals with 0.06 and 0.12 per layer deformation-fault probabilities. Note that the diffraction peaks have been slightly displaced from their Bragg's law positions of $l = -\frac{2}{3}, \frac{1}{3}$. The displacement obtained is in agreement with the analytical calculations of Hirsch & Otte (1957). Fig. 5(*c*) contains the calculated diffraction profile for a more complicated layer defect, a two-layer twin fault. The jogs of g_n in this case are equivalent to those shown in Fig. 2(*a*) occurring at random, rather than regular, positions. This model exhibits strong asymmetric streaking as well as a significant diffraction-peak-position shift in the direction opposite to that produced by simple deformation faults.

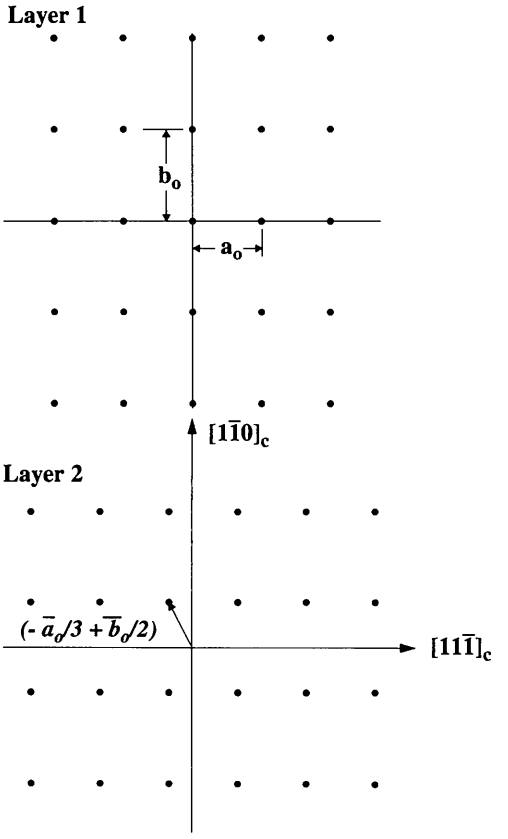

Fig. 4. The positions for atoms on two successive (211) layer planes, denoted layer 1 and layer 2, that form a b.c.c. crystal. Six layers comprise the complete unit cell. The orientation of the cubic $[1\bar{1}0]$ and $[11\bar{1}]$ directions is shown, as is the vector representing the displacement between successive layers in the perfect crystal stacking.

5. Summary

This contribution illustrates a particularly facile method for calculating the diffraction profiles for

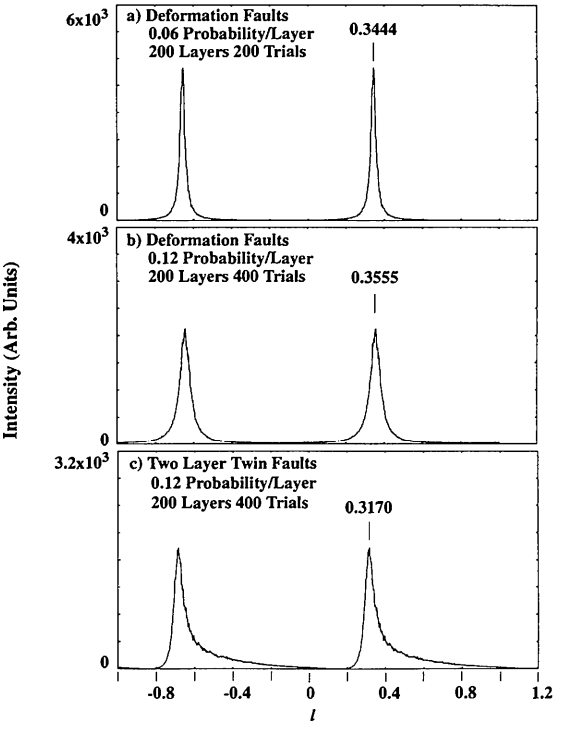

Fig. 5. Calculated b.c.c. diffraction profiles. In each case, the intensity has been calculated along the orthorhombic 10*l* line for ensembles of either 200 or 400 crystallites. (*a*) Deformation faults, 0.02 probability per layer. (*b*) Deformation faults, 0.12 probability per layer. (*c*) Two-layer twin faults, 0.12 probability per layer. The position of the peak of the intensity distribution is indicated for each distribution.

crystals with layer defects. Its primary utility is that complex defect models can be easily analyzed in comparison with experimental results. Three cases have been presented as examples: stacking faults in the Ni_xAl_{1-x} $(5, \bar{2})$ monoclinic martensite, layer defects in trigonal polytypes and faults in the (211) planes of a b.c.c. crystal. In each case, the position of the nth layer is expressed in terms of a phase index, g_n, which is then tabulated for an ensemble of crystallites. The averages that prescribe the diffracted intensity profile are then evaluated by direct computation. The parameters of the calculation, the size of the crystallite N_c and the number of crystallites in the ensemble T can be empirically determined. In some cases, N_c or T may be specified by the nature of the problem: for instance, a small value of N_c might be used to analyze the diffraction patterns obtained from thin adsorbed gas layers on surfaces. An appropriate value for T can usually be obtained by numerical experimentation.

Implementation of diffraction-profile calculations such as these requires rather simple computer programs. The b.c.c. (211)-plane example is less than 100 lines of Fortran code exclusive of comments and calculates 2000 values of $I(l)$ for an ensemble of 200 crystallites 100 layers long in less than 2 min on a DEC MicroVAXIII+. Copies of the computer programs appropriate to the $7M$, b.c.c. and trigonal cases discussed in this paper are available from one of the authors.* Extension of these ideas to layer defects in crystals with variable layer spacing or to crystals composed of different kinds of layers appears to be straightforward.

The authors gratefully acknowledge the assistance of Y. Noda, who provided a copy of the raw data from his neutron diffraction experiments on Ni_xAl_{1-x}. The authors also acknowledge the helpful comments of M. Popovici, who read a draft of the manuscript.

* R. Berliner, Research Reactor Center, University of Missouri, Columbia, MO 65211, USA. (e-mail: Berliner@murrvax).

References

BACON, G. E. (1975). *Neutron Diffraction*. Oxford: Clarendon Press.

BARRETT, C. & MASSALSKI, T. B. (1980). *Structure of Metals*. New York: Pergamon Press.

BARSCH, G. R. & KRUMHANSL, J. A. (1988). *Metall. Trans. A*, **19A**, 761–774.

BERLINER, R., FAJEN, O., SMITH, H. G. & HITTERMAN, R. L. (1989). *Phys. Rev. B*, **40**, 12086–12097.

BERLINER, R., SMITH, H. G., COPLEY, J. R. D. & TRIVISONNO, J. (1992). *Phys. Rev. B*, **46**, 14436–14447.

BERLINER, R. & WERNER, S. A. (1986). *Phys. Rev. B*, **34**, 3586–3603.

GOODING, R. J. (1989). *Phys. Rev. B*, **40**, 4157–4159.

GUENTERT, O. J. & WARREN, B. E. (1958). *J. Appl. Phys.* **29**, 40–48.

GUINIER, A. (1963). *X-ray Diffraction*. San Francisco, London: W. H. Freeman.

HENDRICKS, S. & TELLER, E. (1942). *J. Chem. Phys.* **10**, 147–167.

HIRSCH, P. B. & OTTE, H. M. (1957). *Acta Cryst.* **10**, 447–453.

JAGODZINSKI, H. (1949). *Acta Cryst.* **2**, 201–206, 208–214, 298–304.

KRIVOGLAZ, M. A. (1969). *Theory of X-ray and Thermal-Neutron Scattering by Real Crystals*. New York: Plenum Press.

LANDAU, L. (1937). *Phys. Z. Sowjetunion*, **12**, 579–585.

LIFSCHITZ, M. (1937). *Phys. Z. Sowjetunion*, **12**, 623–643.

LIFSCHITZ, M. (1939). *Zh. Eksp. Teor. Fiz.* **9**, 500–511.

MARTYNOV, V. Y., ENAMI, K., KHANDROS, L. G., NENNO, S. & TKACHENKO, A. V. (1983). *Phys. Met. Metallogr. (USSR)*, **55**, 136–143.

NODA, Y., SHAPIRO, S. M., SHIRANE, G., YAMADA, Y. & TANNER, L. E. (1990). *Phys. Rev. B*, **42**, 10397–10404.

ROTHMAN, R. L. & COHEN, J. B. (1971). *J. Appl. Phys.* **42**, 971–979.

SCHWARTZ, L. H. & COHEN, J. B. (1977). *Diffraction from Materials*. Berlin: Springer Verlag.

SHAPIRO, S., YANG, B. X., NODA, Y., TANNER, L. E. & SCHRYVERS, D. (1991). *Phys. Rev. B*, **44**, 9301–9313.

VERMA, A. R. & KRISHNA, P. (1986). *Polymorphism and Polytypism in Crystals*. New York: Wiley.

WARREN, B. E. (1969). *X-ray Diffraction*. Reading, MA: Addison-Wesley.

WELBERRY, T. R. (1985). *Rep. Prog. Phys.* **48**, 1543–1593.

WILSON, A. J. C. (1941). *Proc. R. Soc. London Ser. A*, **180**, 277–285.

WILSON, A. J. C. (1949). *X-ray Optics*. New York: Wiley.

YAMADA, Y., NODA, Y. & FUCHIZAKE, K. (1990). *Phys. Rev. B*, **42**, 10405–10414.